© 2017. Published by The Company of Biologists Ltd | Journal of Cell Science (2017) 130, 132-142 doi:10.1242/jcs.187815

SPECIAL ISSUE: 3D CELL BIOLOGY

RESEARCH ARTICLE

Morphological process of podocyte development revealed by block-face scanning electron microscopy

Koichiro Ichimura[1,*], Soichiro Kakuta[2], Yuto Kawasaki[1], Takayuki Miyaki[1], Takahiro Nonami[1], Naoyuki Miyazaki[3], Tomoyo Nakao[4], Sakiko Enomoto[4], Shigeo Arai[4], Masato Koike[5], Kazuyoshi Murata[3] and Tatsuo Sakai[1]

ABSTRACT

Podocytes present a unique 3D architecture specialized for glomerular filtration. However, several 3D morphological aspects on podocyte development remain partially understood because they are difficult to reveal using conventional scanning electron microscopy (SEM). Here, we adopted serial block-face SEM imaging, a powerful tool for analyzing the 3D cellular ultrastructure, to precisely reveal the morphological process of podocyte development, such as the formation of foot processes. Development of foot processes gives rise to three morphological states: the primitive, immature and mature foot processes. Immature podocytes were columnar in shape and connected to each other by the junctional complex, which migrated toward the basal side of the cell. When the junctional complex was close to the basement membrane, immature podocytes started to interdigitate with primitive foot processes under the level of junctional complex. As primitive foot processes lengthened, the junctional complex moved between primitive foot processes to form immature foot processes. Finally, the junctional complex was gradually replaced by the slit diaphragm, resulting in the maturation of immature foot processes into mature foot processes. In conclusion, the developmental process of podocytes is now clearly visualized by block-face SEM imaging.

KEY WORDS: Block-face imaging, Glomerulus, Glomerulogenesis, Podocyte

INTRODUCTION

Podocytes are highly complex epithelial cells that are specialized for glomerular ultrafiltration. In older textbooks, podocytes are said to be composed of three kinds of subcellular compartments, the cell body, primary process and foot process (Fig. S1A1) (Kriz and Kaissling, 2000; Ichimura and Sakai, 2015). The cell body of the podocyte projects five to ten primary processes, and each primary process protrudes numerous foot processes. Podocytes interdigitate with each other and adhere to the glomerular basement membrane (GBM) through the foot processes to form a glomerular epithelium (Fig. S1D1-2). The intercellular junction of podocytes, which is called the 'slit diaphragm' spans between the foot processes. The slit diaphragm and the GBM mainly prevent the leakage of plasma protein into the primary urine.

Conventional scanning electron microscopy (SEM) is a useful method to explore the unique three-dimensional architecture of podocytes, as their large luminal surface faces the urinary space of the Bowman's capsule (Fujita et al., 1970; Andrews and Porter, 1974; Bulger et al., 1974; Inokuchi et al., 1996). However, conventional SEM is not sufficient to reveal the whole architecture of individual podocytes because this method does not allow the direct observation of the basal surface of podocytes and some parts of podocytes situated within the deep vales, which are formed between the glomerular capillary loops. To overcome these problems and to reveal the architecture of podocytes, we recently examined three-dimensional reconstruction images of podocytes; these images were based on serial cross-sectional images acquired by block-face SEM imaging (Ichimura et al., 2015). This SEM technique enables the efficient acquisition of a series of transmission electron microscopy (TEM)-like images directly from resin-embedded biological samples (Ohta et al., 2012; Kubota, 2015; Ohno et al., 2015).

Our recent analysis of the reconstruction images revealed that a more accurate structural hierarchy of podocyte subcellular compartments includes 'ridge-like prominences' (Fig. S1A2), which are protruded directly from the basal surface of the cell body and primary processes (Fig. S1B1-2,C1-2). The ridge-like prominences serve as an adhesion apparatus for the direct attachment of cell body and primary processes to the GBM, and as a connecting apparatus to link foot processes to cell body or primary processes (Takahashi-Iwanaga, 2002; Burghardt et al., 2015; Ichimura et al., 2015).

Such a unique architecture of podocytes is formed during the glomerular development. Immature podocytes, which initially form a simple columnar epithelium, exhibit several alterations to form the mature podocytes, as summarized in Fig. 1 (Reeves et al., 1978). The intercellular junctions between immature podocytes initially consist of a tight and adherence junction complex (Fig. 1A1–3). During development, the tight and adherence junction complex moves toward the basal side of the cell (Fig. 1B1–3) and, then, podocytes become vigorously interdigitated each other with their foot processes (Hartleben et al., 2012) (Fig. 1C1–3). The tight and adherence junction complex localizes between the foot processes and finally it becomes almost completely replaced by the slit diaphragm (Fig. 1D1–3). The outline of the morphological process in podocyte development is understood as mentioned above. However, some morphological aspects that are difficult to reveal by conventional electron microscopy remain only fragmentarily understood (Quaggin and Kreidberg, 2008).

In the present study, we examined the podocyte development in neonatal rat kidney by using serial block-face SEM imaging and

[1]Department of Anatomy and Life Structure, Juntendo University Graduate School of Medicine, Tokyo 113-8421, Japan. [2]Laboratory of Morphology and Image Analysis, Center for Biomedical Research Resources, Juntendo University Graduate School of Medicine, Tokyo 113-8421, Japan. [3]National Institute for Physiological Sciences, Okazaki 444-8585, Japan. [4]High Voltage Electron Microscope Laboratory, Nagoya University, Nagoya 464-8603, Japan. [5]Department of Cell Biology and Neuroscience, Juntendo University Graduate School of Medicine, Tokyo 113-8421, Japan.

*Author for correspondence (ichimura@juntendo.ac.jp)

K.I., 0000-0001-6590-7912

Received 15 February 2016; Accepted 20 June 2016

Journal of Cell Science

Journal of Cell Science (2017) 130, 132-142 doi:10.1242/jcs.187815

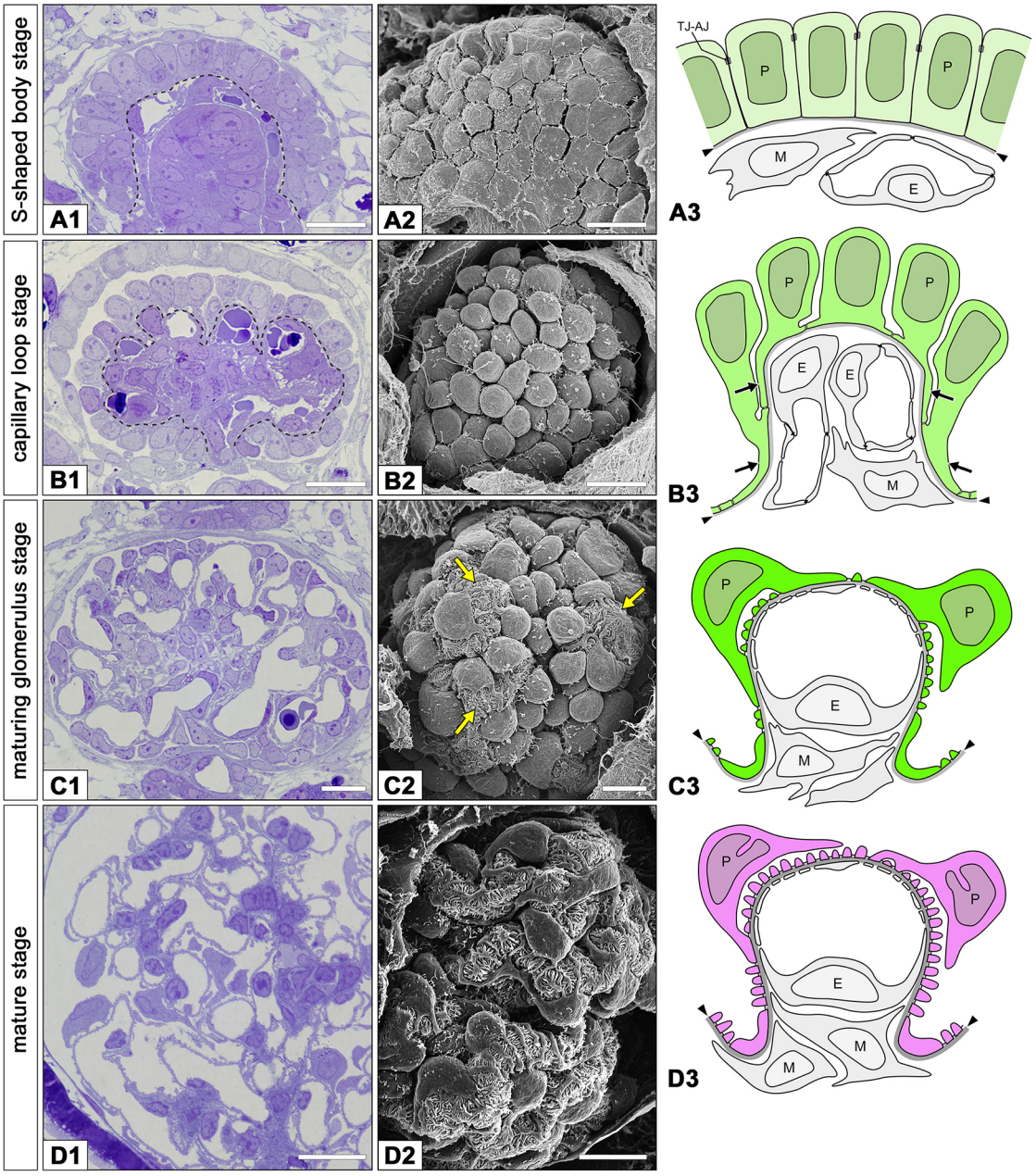

Fig. 1. Outline of glomerulus development. (A1–D1) Toluidine-Blue-stained semi-thin sections. (A2–D2) Conventional SEM. (A3–D3) Schematic representations highlighting the podocyte development. (A1–3) S-shaped body stage. Podocytes form a simple columnar epithelium. The luminal surface of glomerulus exhibited a cobblestone appearance. Primitive glomerular capillaries and mesangial cells were already detected beneath the GBM, dotted line. (B1–3) Capillary loop stage. Primitive glomerular capillaries and mesangium had developed and invaginated into the epithelial layer formed by podocytes and GBM (dotted line). Intercellular junctions moved close to the GBM and then the luminal surface of the glomerulus exhibited a shape similar to a stalk of a grape. The lateral surface of capillary walls was covered with the tongue-like portion of the podocyte cell body (arrows in B3). (C1–3) Maturing glomerulus stage. The simple glomerular capillaries became more complicated. The intercellular space between podocyte cell bodies widened. As a result, the glomerular wall was covered by the immature primary and foot processes, which were visible in conventional SEM (arrows in C2). (D1–3) Mature stage. The mesangium became highly arborized. Podocytes covered the urinary surface of the GBM mainly with their numerous mature foot processes. E, glomerular endothelial cell; M, mesangial cell; P, podocyte. Arrowheads, GBM. Scale bars: 10 µm.

three-dimensional reconstruction. We were successful at describing the morphological process of podocyte development more clearly and precisely than ever before.

RESULTS

Glomerulus development is morphologically divided into seven stages in the mammalian metanephric kidney, including condensation, renal vesicular, comma-shaped body, S-shaped body, capillary loop, maturing glomerulus and mature stages (Reeves et al., 1978; Little et al., 2007; Georgas et al., 2009). Morphological alteration of podocytes vigorously progresses, especially from the S-shaped body to maturing glomerulus stages, as shown in Fig. 1. We thus examined the podocytes during this period.

We obtained serial block-face SEM images from kidney samples using two types of SEM, a focused ion beam SEM (FIB-SEM) (Heymann et al., 2006; Knott et al., 2011) and a serial block face-

Journal of Cell Science (2017) 130, 132-142 doi:10.1242/jcs.187815

SEM (SBF-SEM) (Denk and Horstmann, 2004; Knott et al., 2008). The three-dimensional reconstruction images based on FIB-SEM and SBF-SEM images were similar in terms of quality (see Fig. 2 and Fig. S2), although the surface of podocytes reconstructed from FIB-SEM images appeared to be smoother than those from SBF-SEM images, because the electrical distortion of each block-face image due to surface charging was less in the FIB-SEM images. In the present study, we mainly demonstrate the reconstruction images based on serial FIB-SEM images.

S-shaped body stage

Individual podocytes presented a polygonal column shape and were connected to each other by the tight and adherence junction complex to form a simple epithelium (Fig. 1A1,A3). Thus, the glomerulus exhibited a cobblestone appearance when observed from the luminal side (Fig. 1A2). However, the basal surface of each reconstructed podocyte was irregular in shape, in comparison with their luminal surface (Figs 2A and 3A,C1), because the podocytes inserted their cytoplasmic protrusions under the neighboring podocytes (arrowheads in Fig. 3B2,D). These cytoplasmic protrusions varied in shape and size and were not associated with the tight and adherence junction complex and slit diaphragm (arrowheads in Fig. 3D).

The tight and adherence junction complex was initially localized above the upper fourth of the cell height, as observed in other columnar epithelial cell types (data not shown). During this stage, the tight and adherence junction complex started moving towards the basal side of the cell. In particular, the tricellular portions of tight and adherence junction complex moved more rapidly than the bicellular portions (arrows in Fig. 3B1,B3). Therefore, the bicellular portion exhibited an inverted U (∩) shape (Fig. S3A–C).

Unlike the typical junctional complex, the tight and adherence junction complex of immature podocytes was a mixture of tight and adherence junctions (Fig. 3E). Desmosomes were not morphologically recognized in our examination, although Garrod and Fleming (1990) have reported that desmosomal proteins (desmoplakins and desmoglein) are localized at the intercellular junction of immature podocytes in murine and human embryos.

Capillary loop stage

Primitive glomerular capillaries and mesangium were developed and had invaginated into the epithelial layer formed by the podocytes and GBM. The GBM therefore exhibited a concave–convex appearance (dotted line in Fig. 1B1).

Early phase

The main body of the tight and adherence junction complex was a ring in shape and had already descended close to the basal surface of the podocyte (Fig. 4A1,2,C1). The upper part of the podocytes became rounded and the luminal surface of the glomerulus looked like a stalk of a grape (Fig. 1B2). On the luminal surface of each podocyte, two or three striations of the tight and adherence junction complex extended from its main body (arrowheads in Fig. 4A1,2,C2,3). These striations were presumably formed by the fusion of the ∩-shaped portion of the tight and adherence junction complex observed at the S-shaped body stage, as shown in Fig. S3.

Below the main body of the tight and adherence junction complex, podocytes interdigitated each other with their several dozen fine processes (Fig. 4). These fine processes adhered to the GBM, like the foot processes of mature podocytes, but the tight and adherence junction complex and slit diaphragm were not recognized between them. We refer to these fine processes as ‘primitive foot processes’ in this study. Some podocytes exhibited a few thick primary process-like processes, which we term ‘primitive primary processes’ (arrows in Fig. 4C1–3).

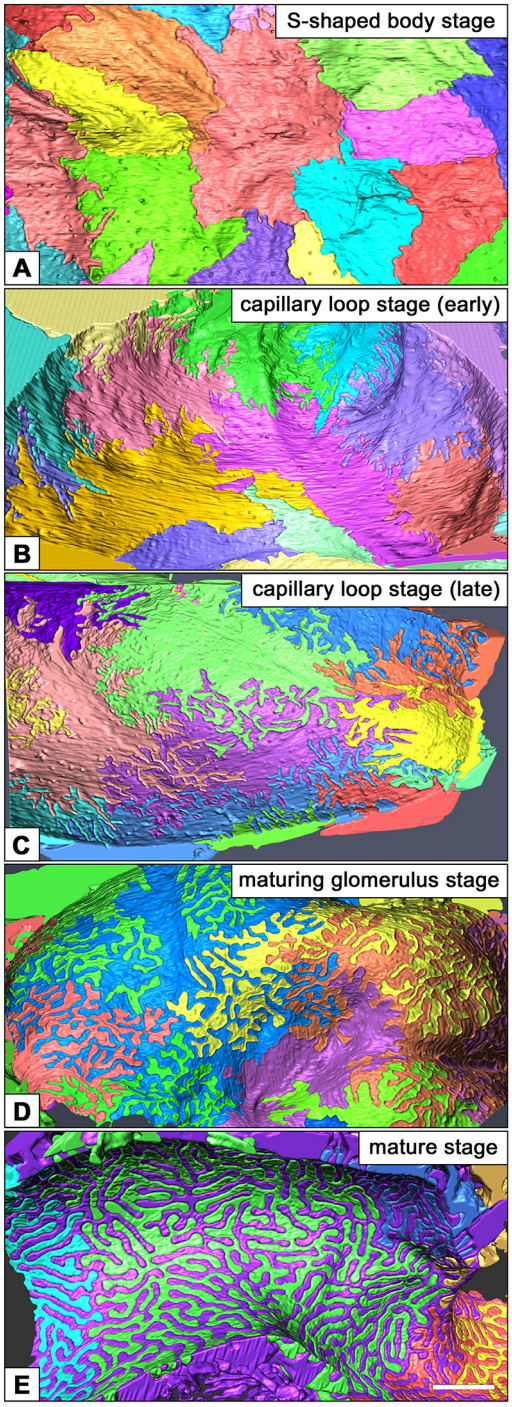

Fig. 2. Basal surface of podocytes reconstructed from serial FIB-SEM images. Individual podocytes are shown in different colors and are viewed from the basal side. In the immature glomerulus, it seems that the number of podocytes covering a certain surface area of GBM is almost constant (A–D). In the completely mature glomerulus, the number of podocytes observed in the same surface area is much smaller (E) because the surface area of GBM is extremely enlarged and each podocyte covers a larger area of the GBM. (A–D) Neonatal rats and (E) adult rats. A similar magnification was used to acquire all images. Scale bar: 2 µm.

Journal of Cell Science (2017) 130, 132-142 doi:10.1242/jcs.187815

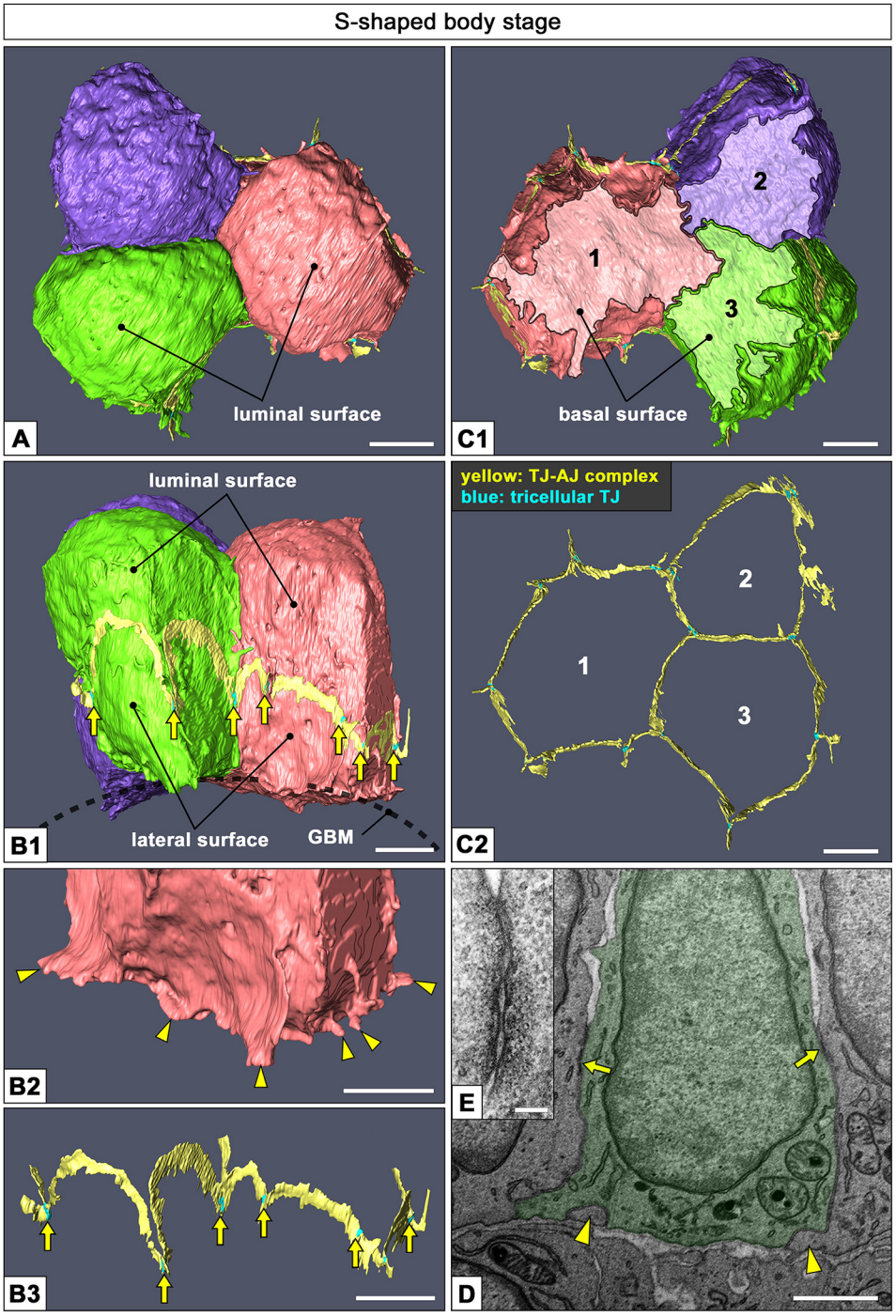

Fig. 3. Podocytes in the late phase of S-shaped body stage. Reconstructed podocytes are viewed from the luminal (A), lateral (B1,2) and basal (C1) sides. Individual podocytes present a polygonal column shape. The top surface of the podocytes was relatively uniform in shape and size (A), as observed in conventional SEM. By contrast, their basal surface is irregular in shape (C1). The isolated junctional structure is also shown from the lateral (B3) and basal (C2) sides. Podocytes are connected to each other by the tight and adherence junction complex (shown in yellow). During this stage, the tight and adherence junction complex is moving towards the basal side of the cell. In particular, the tricellular junctions (shown in blue) moved more rapidly than the tight and adherence junction complex (arrows in B1, B3). Podocytes inserted cytoplasmic protrusions, which are irregular in shape, under the neighboring podocytes (arrowheads in B2). These protrusions were not associated with the tight and adherence junction complex and slit diaphragm (arrowheads in D). Arrows in D, tight and adherence junction complex. Unlike the typical junctional complex, the tight and adherence junction complex is a mixture of tight and adherence junctions in the immature podocytes (E). D, FIB-SEM block-face image; E, conventional TEM image. Scale bars: 2 µm (A–D); 100 nm (E).

Late phase

With the development of glomerular capillaries, the podocyte cell body was pushed up by the neighboring one, while maintaining the original adhesion site to the GBM, resulting in the formation of a ‘tongue-like’ portion of cell body (arrows in Fig. 1B3).

The periphery of the tongue-like portion formed several primitive primary processes (arrows in Fig. 5A,B1,C). Moreover, the primitive primary processes also protruded directly from cell body regions other than the tongue-like portion (Fig. 5A). The primitive foot processes protruded from the primitive primary processes (Fig. 5A,B1,C), and were inserted beneath the primitive primary processes of neighboring podocytes (Fig. 5D1–3,E). Some primitive foot processes bifurcated once or twice (Fig. 5B1,C). The tight and adherence junction complex was located along the transitional portions between the primitive primary and primitive foot processes (Fig. 5C,D1–3). The striations of the tight and adherence junction complex remained on the luminal surface of the cell body (green arrowheads in Fig. 5B1,2,C).

Maturing glomerulus stage

As the simple glomerular capillary loops became more complicated, the intercellular space between podocyte cell bodies widened (Fig. 1C1–3). The outline of reconstructed podocytes was similar to that observed at the mature stage. The primary and foot processes were short in length and irregular in shape, in comparison with those of mature podocytes (Fig. 6A1,2). The primary and foot processes

Journal of Cell Science (2017) 130, 132-142 doi:10.1242/jcs.187815

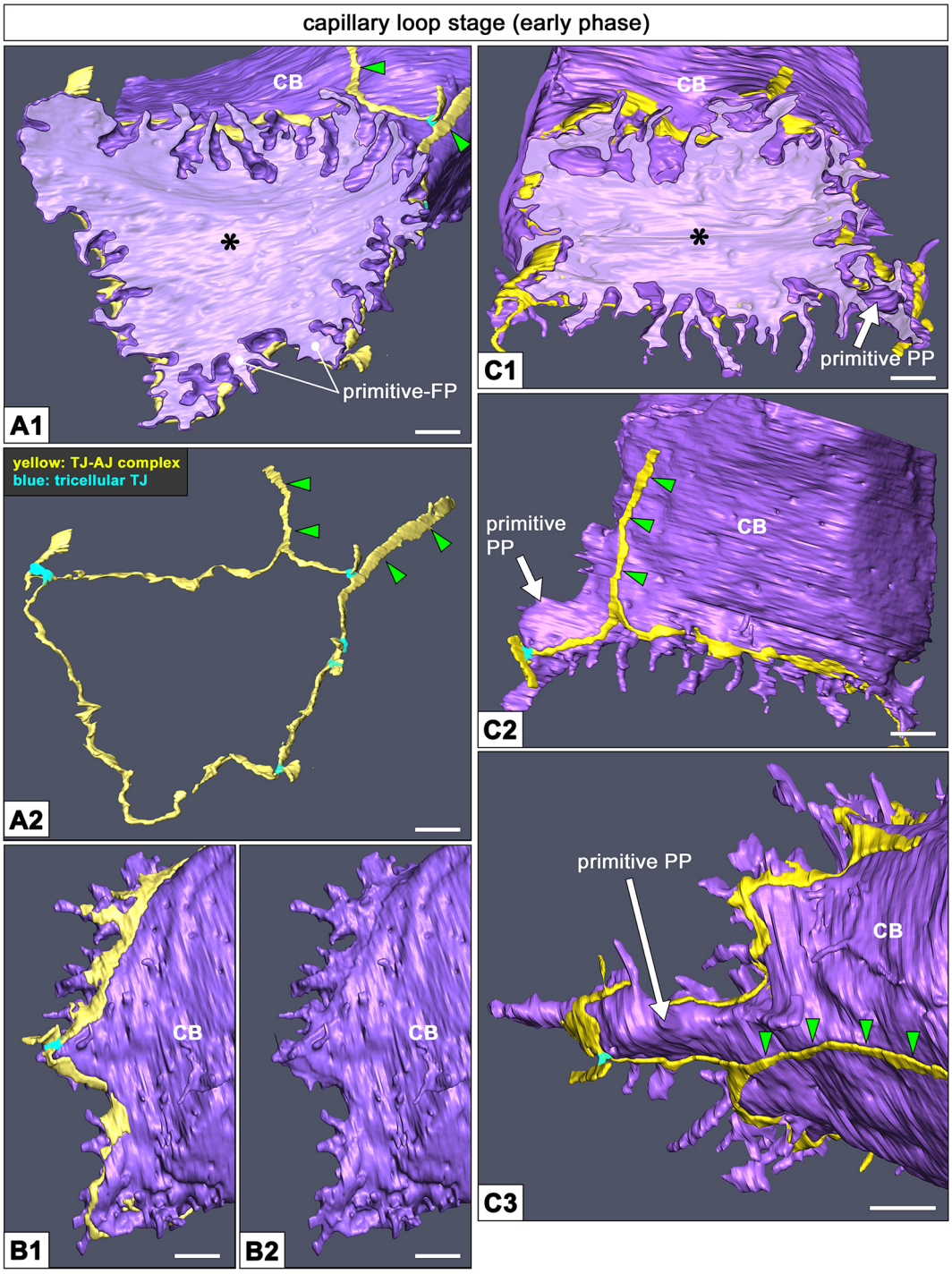

Fig. 4. Podocytes in the early phase of capillary loop stage. Cellular interdigitation is vigorously formed by the primitive foot processes (primitive-FP in A1). The tight and adherence junction complex is localized just above the primitive foot processes, but not between them (B1, B2). In some podocytes, the primitive primary processes are already formed (primitive PP in C1–3). The striations of the tight and adherence junction complex extended from the ring of the tight and adherence junction complex (arrowheads in A2, C2, C3). As observed in the S-shaped body stage, the primitive foot processes did not associated with the tight and adherence junction complex and slit diaphragm. Asterisk, basal surface of podocyte; CB, cell body. Scale bars: 500 nm.

still exhibited immaturity at this stage, we thus refer to them as immature primary and immature foot processes in this study to distinguish them from the completely mature forms.

The immature primary processes within individual podocytes exhibited various degrees of development. Some of them adhered to the GBM through a relatively large area (Fig. 6A2–4). Others had already formed a ridge-like prominence as observed in the mature podocytes (Fig. 6A5). Podocytes inserted their immature primary processes under the cell bodies of neighboring podocytes, resulting in the separation of the cell body from the GBM to form the subpodocyte space (Neal et al., 2005) (Fig. 6A2).

The tight and adherence junction complex was localized between the immature foot processes and it was partially replaced by the slit diaphragm (Fig. 6B1,2). The striations of the tight and adherence

Journal of Cell Science (2017) 130, 132-142 doi:10.1242/jcs.187815

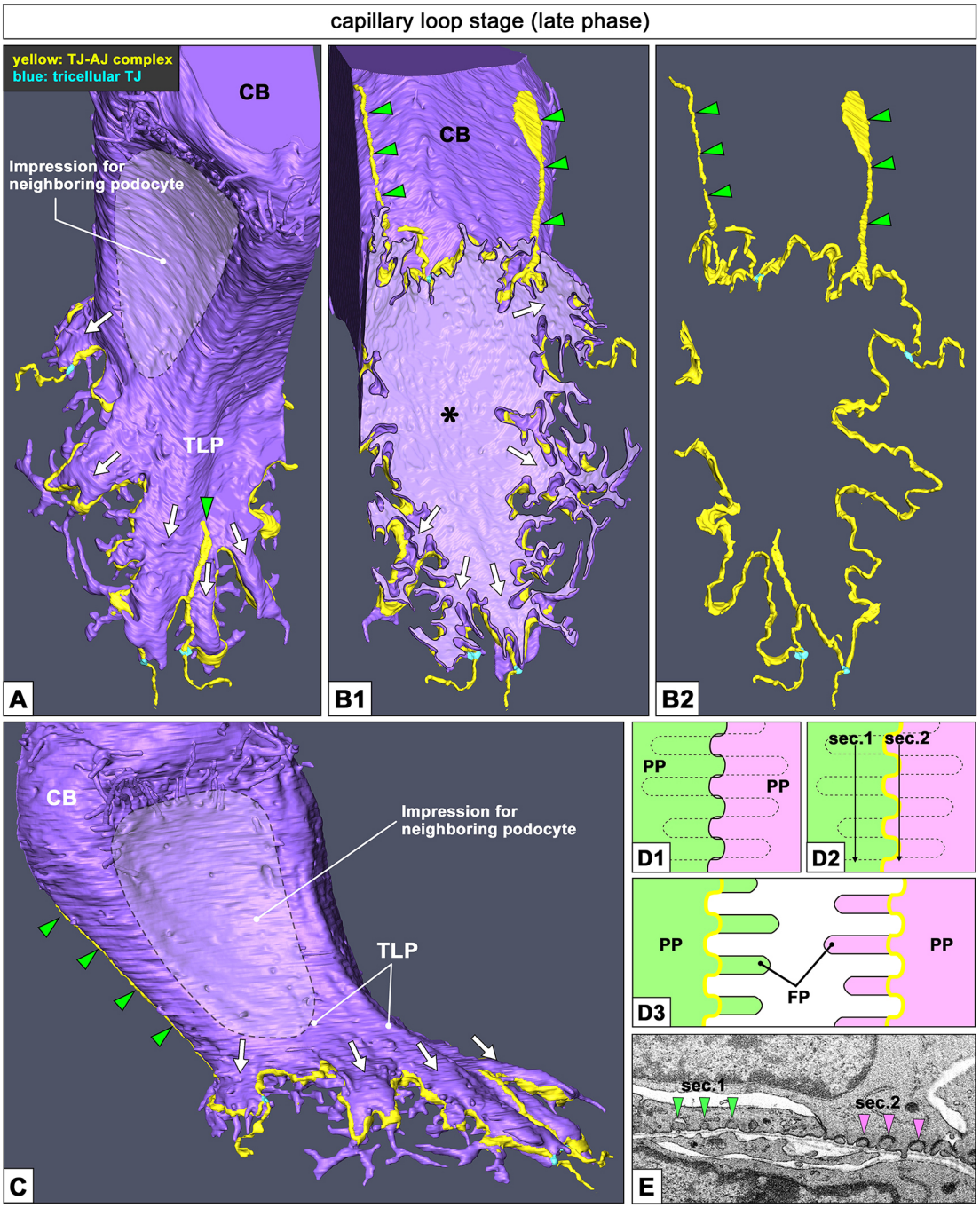

Fig. 5. Podocytes in the late phase of capillary loop stage. (A) The primitive primary processes (arrows in A–C) are vigorously protruded from the cell body (CB), including the tongue-like portion (TLP), and are fringed with the tight and adherence junction complex. (B1,2) The primitive primary processes adhered to the GBM with a broad area or a ridge-like prominence, as observed in the mature podocytes (see Fig. S1). On the luminal surface of the podocyte cell body, the striations of the tight and adherence junction complex extend from the ring of the tight and adherence junction complex (green arrowheads in A–C). (C) The ring of the tight and adherence junction complex was localized along the periphery of primitive primary processes. Asterisk in A, basal surface of podocyte. (D1–3) Schematic drawings illustrating the location of the tight and adherence junction complex. Two neighboring primitive primary processes (PP) are shown in green and red, and are viewed from the luminal side (D1). The primitive foot processes are inserted beneath the neighboring primitive primary processes (dotted lines in D1). The location of the tight and adherence junction complex is shown by the yellow line in the adhering (D2) and separated (D3) podocytes. The primitive primary processes are fringed with the tight and adherence junction complex. The distal portion of the primitive foot processes (FP in D3) is not associated with the tight and adherence junction complex. (E) Block-face image. The cross sections at the lines in D2 (sec.1, sec.2) are shown. The green arrowheads indicate the distal portion of the primitive foot processes. The pink arrowheads indicate the transitional portions between the primitive primary and the primitive foot processes. Scale bar: 1 µm.

junction complex almost disappeared at this stage, although a patchy tight and adherence junction complex remained between the cell bodies or between the immature primary processes in a few cells.

In some podocytes, the tongue-like portion of the cell body remained and exhibited a large fenestration (Fig. S4A1,2). In mature podocytes, the distal portions of two primary processes originating

Journal of Cell Science (2017) 130, 132-142 doi:10.1242/jcs.187815

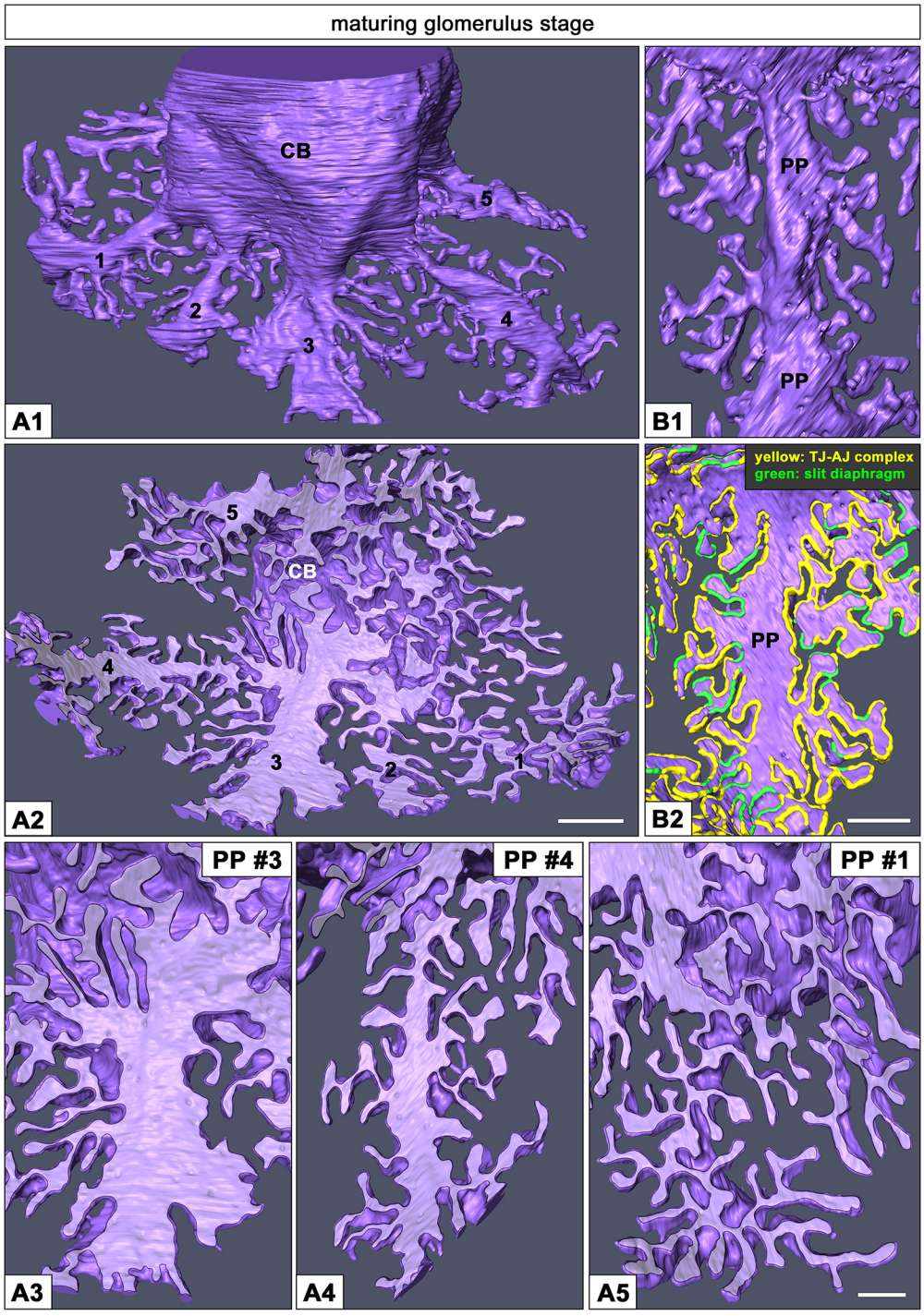

Fig. 6. Podocytes in the maturing glomerulus stage. The overall image of the podocyte is similar to that observed during the mature stage (A1), although the immature primary processes (nos 1–5 in A1, A2) are still short in length and irregular in shape. (A3–5) The basal surface of three immature primary processes (nos 1, 3, 4) shown in A2 are magnified in A3, A4 and A5. The developmental degree is different among the processes. Some immature primary processes exhibit a relatively large adhesive surface to the GBM (A3, A4), but others already form a ridge-like prominence to adhere to the GBM (A5) as observed in mature podocytes (see Fig. S1). The tight and adherence junction complex is localized between the immature foot processes and is partially replaced by the slit diaphragm (B1, B2). CB, cell body; PP, immature primary process. Scale bars: 1 µm (A2); 500 nm (A5, B2).

from the same cell were sometimes anastomosed to form a cytoplasmic arcade (see next section, Fig. S4B). This arcade is highly likely to be formed from the fenestrated tongue-like portions because of an enlargement of its fenestration.

Mature stage

The cell bodies of podocytes were largely separated from each other, and the mature primary and foot processes were easily visible by conventional SEM (Fig. 1D2). The mature primary and foot processes were more extended and thickened when compared to the immature primary and foot processes observed in the former stage. Moreover, the mature foot processes were uniform in width when compared to the primitive and immature foot processes (Figs 2 and 7).

The cytoplasmic arcade of primary processes is a newly identified structure in this study (Fig. S4B). These arcades were often situated within the vales, which are formed between the glomerular capillary loops. Thus, it was difficult to visualize them by conventional SEM.

The tight and adherence junction complex between the foot processes was almost completely replaced by the slit diaphragm, although a few patchy tight junctions were found between the foot processes in mature podocytes (arrowheads in Fig. S1D2), consistent with the findings of Rodewald and Karnovsky (1974).

Journal of Cell Science (2017) 130, 132-142 doi:10.1242/jcs.187815

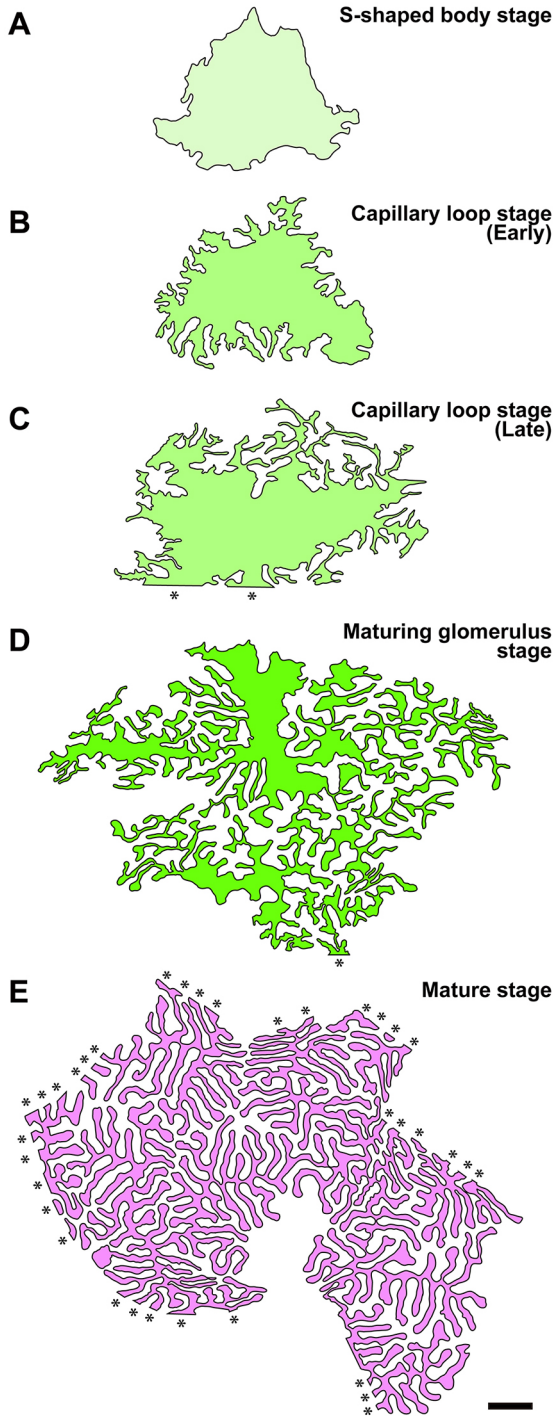

Fig. 7. Developmental alterations of the basal surface structure in podocytes. The planar projection of the podocyte basal surface is shown at each developmental stage. During immature stages, the entire or almost entire basal surface of one podocyte can be shown (A–D). During the mature stage, only one part of the basal surface area is shown, because the area covered by one podocyte is quite enlarged (E). The basal surface of mature foot processes is regular in shape in comparison with that of primitive (B,C) and immature (D) foot processes. A similar magnification was used in all figures. Asterisks, cut edge. Scale bar: 1 µm.

The tight junctions also remained at the tricellular junctions, where the slit diaphragm was not formed (arrows in Fig. S1D1,2). The striations of the tight and adherence junction complex disappeared, and the podocyte cell bodies became largely separated.

DISCUSSION

The morphological process of podocyte development has been widely examined to reveal the mechanism by which the unique architecture of podocytes is established. Conventional SEM is helpful to three-dimensionally reveal the outline of this process (Miyoshi et al., 1971; Spinelli, 1974; Hay and Evan, 1979; Iino et al., 2001). However, the podocyte process formation in development is indeed difficult to visualize by this method, because it progresses under the cell bodies that are closely spaced to each other during the early stage of development. Therefore, only patchy information has been available on the morphology of the podocyte process formation until now. In the present study, using FIB-SEM imaging and a reconstruction technique, the podocyte process formation was more clearly and precisely detailed from the relationship with their intercellular junctions (as summarized in Fig. 8A). The foot processes presented three developmental states: primitive, immature and mature foot processes (Fig. 8B). Once the tight and adherence junction complex moved closer to the GBM, podocytes started to interdigitate with primitive foot processes. Subsequently, the short primitive primary processes were developed and inserted beneath the neighboring podocyte cell body. As the primitive foot and primitive primary processes grew, the tight and adherence junction complex moved between the primitive foot processes to form the immature primary and foot processes. Finally, the tight and adherence junction complex was almost completely replaced with the slit diaphragm to form the mature foot processes.

In general, the intercellular junctional complexes between epithelial cells were subdivided into one of two forms, bicellular and tricellular junctions (Furuse et al., 2014). The structure and molecular components have been extensively investigated for the bicellular junction of podocytes, including the slit diaphragm (Patrakka and Tryggvason, 2010; Scott and Quaggin, 2015). However, no information on the tricellular junction of podocytes had been reported previously. Our analysis provides some findings on podocyte tricellular junctions. During the early development of podocytes, the descending rate of tricellular junctions was quicker than that of bicellular junctions, suggesting that the tricellular junctions play a role in leading the movement of the tight and adherence junction complex. In other epithelial cells, molecular components of tricellular tight junctions are known, such as the tricellulin (also known as MARVELD2) transmembrane protein (Ikenouchi et al., 2005) and angulin family transmembrane proteins (Higashi et al., 2013; Iwamoto et al., 2014). Examination of the post-transcriptional modification of tricellular junction proteins might provide information useful to determine the mechanism underlying the movement of the tight and adherence junction complex in podocytes.

Expression and localization of intercellular junctional proteins are dynamically altered in podocytes under developmental and disease conditions (Yaoita et al., 2002a,b; Usui et al., 2003; Quaggin and Kreidberg, 2008; Koda et al., 2011). Serial block-face SEM imaging allows the analysis of three-dimensional protein localization by the use of pre-embedding immunogold labeling and enhancement techniques (Sonomura et al., 2013). In combination with the present findings, the information on three-dimensional localization of junctional proteins should be valuable to understanding of the mechanisms underlying the developmental formation of the slit diaphragm. However, in our preliminary experiment for this analysis, there were some technical drawbacks. One of the major problems was the difficulty to obtain a uniform labeling with the antibody. Future studies are warranted to overcome

Journal of Cell Science (2017) 130, 132-142 doi:10.1242/jcs.187815

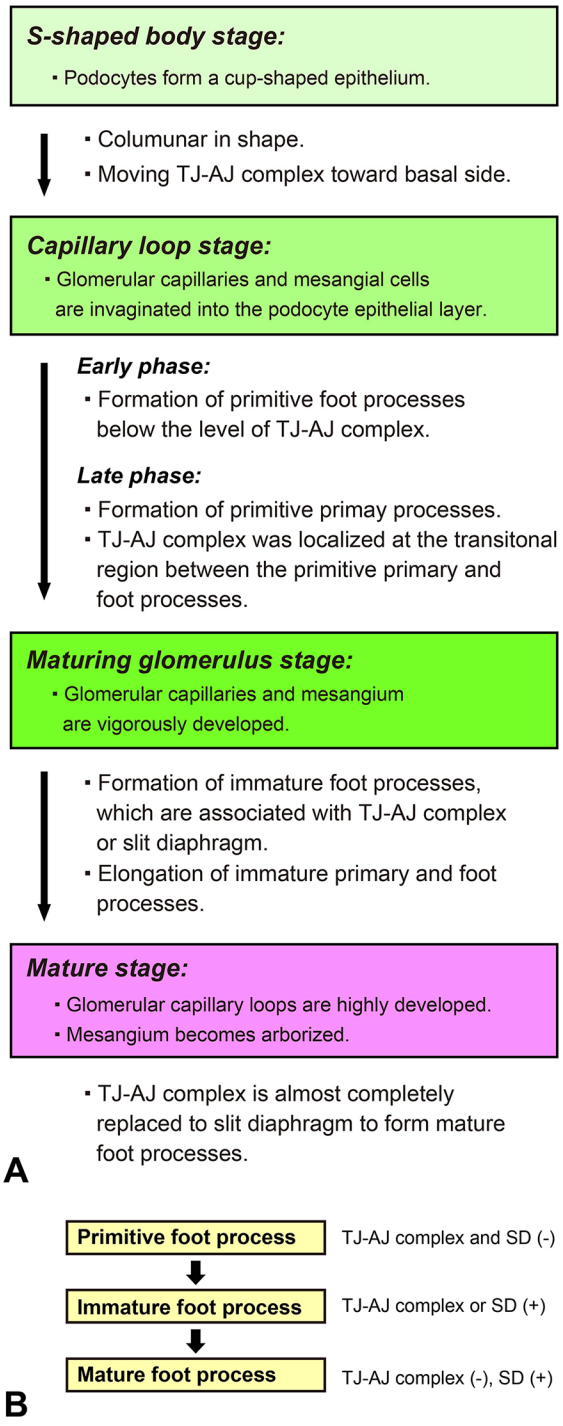

Fig. 8. Diagram of podocyte development. (A) Morphological alterations of podocytes are summarized for each developmental stage. Major characteristics of other glomerular structures are listed in the rectangles. (B) The development of foot processes presents three morphological states, the primitive, immature and mature foot processes, which are defined in relation to the junctional structures.

these problems and to analyze the three-dimensional alteration of junctional protein localization in developing podocytes.

In the present study, we used two types of SEM (FIB-SEM and SBF-SEM) to obtain the serial block-face images. The reconstruction images of podocytes based on the FIB-SEM and SBF-SEM images were of sufficient quality to allow analysis of their three-dimensional structure. However, the surface of the reconstructed podocytes appeared slightly irregular in SBF-SEM images in comparison with that on FIB-SEM images, because the electrical distortion of each block-face image due to surface charging was larger in the SBF-SEM images. Recently, Nguyen and colleagues (2016) have reported that a type of conductive resin containing the carbon black filler, Ketjen Black, prevented surface charging during serial block-face imaging of kidney and brain samples by SBF-SEM.

In conclusion, the serial block-face SEM imaging was useful to understand the three-dimensional architecture of podocytes, which was difficult to visualize by conventional TEM and SEM alone. Using this method, we could describe and analyze the morphological process of podocyte development in more detail than ever before.

MATERIALS AND METHODS

Animal preparation

Postnatal (1-day-old) and adult (10-weeks-old, male) Wistar rats (Charles River Japan, Yokohama, Japan) were used for the examination of immature and mature podocytes, respectively. Animals were perfused with physiological saline and subsequently 2.5% glutaraldehyde fixative buffered with 0.1 M phosphate buffer under anesthesia with pentobarbital. All procedures performed on laboratory animals were approved by the Institutional Animal Care and Use Committee of Juntendo University School of Medicine (approval no. 250042). All animal experiments were carried out in accordance with the Guidelines for Animal Experimentation of Juntendo University School of Medicine.

Conventional SEM

Conventional SEM was performed as previously described (Dong et al., 2010). In brief, small cubes of fixed kidney cortex were immersed in 2% osmium tetroxide in 0.1 M PB for 2 h. After dehydration with a graded series of ethanol, specimens were transferred to *t*-butyl alcohol, and freeze-dried with an ES-2030 freeze dryer (Hitachi High-Technologies, Tokyo, Japan). After mounting on aluminium stubs with carbon paste, the dried specimens were coated with osmium with an OPC80T osmium plasma coater (Filgen, Nagoya, Japan) and observed with an S-4800 field-emission scanning electron microscope (Hitachi High-Technologies).

Conventional TEM

Conventional TEM was performed as described previously (Ichimura et al., 2007, 2010). In brief, the fixed kidney samples were cut into 250-µm-thick sections with a DTK-1000 Microslicer (Dosaka EM, Kyoto, Japan). The sections were successively immersed in 0.4% OsO_4 in 0.1 M phosphate buffer for 1 h, followed by 2% low-molecular-mass tannic acid (Electron Microscopy Sciences, Hatfield, PA, USA) in 0.05 M maleate buffer for 3 h, and 1% uranyl acetate in 0.05 M maleate buffer for 3 h. The samples were then dehydrated in a graded series of cold acetone, and embedded in epoxy resin (Oken Epok 812; Oken-shoji, Tokyo, Japan). Ultrathin silver-gold sections were cut with a diamond knife, transferred to copper grids (50 mesh) that had been coated with Formvar membrane, stained with uranyl acetate and lead citrate, and observed with a JEM1230 transmission electron microscope (JEOL, Tokyo, Japan).

Sample preparation for serial block-face imaging

The fixed kidney samples were cut into 250-µm-thick slices with a DTK-1000 Microslicer, and the slices were processed largely in accordance with the combinatorial heavy metal staining protocol which has been released on the website of the National Center for Microscopy and Imaging Research (La Jolla, CA; http://ncmir.ucsd.edu/sbfsem-protocol.pdf). This protocol was designed to enhance signal for backscatter electron imaging of epoxy-resin-embedded mammalian tissues at low accelerating voltages. In brief, the tissue slices were successively immersed in 1% osmium tetroxide containing 1.5% potassium ferrocyanide in 0.1 M cacodylate buffer for 1 h on ice, 1% low-molecular-mass tannic acid (Electron Microscopy Sciences) in 0.1 M cacodylate buffer for 4 h at room temperature, 2% aqueous osmium

tetroxide for 30 min at room temperature, 1% aqueous uranyl acetate overnight at room temperature, and Walton's lead aspartate solution for 30 min at 60°C. The slices were then dehydrated with a graded series of ethanol, and were embedded in Oken Epok 812.

Serial block-face imaging by FIB-SEM

The surface of resin-embedded tissues was exposed using a diamond knife on an Ultracut UCT (Leica Microsystems, Vienna, Austria). The blocks were mounted onto an aluminium stub and then coated with a thin layer of heavy metal to prevent charging. The surface of embedded tissue was imaged with a Helios Nanolab 650 FIB-SEM (FEI, Eindhoven, The Netherlands) or an MI4000L FIB-SEM (Hitachi High-Technologies) at a high acceleration voltage of 20 kV to find the area of interest. New surface for serial block-face imaging was generated by FIB milling at a 0.77 nA beam current, where gallium ions were accelerated by a voltage of 30 kV. Serial block-face images were obtained every 50-nm depth with a backscattered electron detector at an acceleration voltage of 1.9 kV. The pixel size was 16.5 nm/pixel wide, 21.0 nm/pixel height, 50 nm/pixel depth, and the pixel dimensions of a recorded image were 3072×2048 pixels or 2048×2048 pixels. The contrast of the images was inversed.

Serial block-face imaging by SBF-SEM

Small pieces of block including glomerulus were trimmed and mounted on aluminium specimen pins (Gatan, Pleasanton, CA, USA) using CircuitWorks Conductive Epoxy (Chemtronics, Kennesaw, GA, USA). The entire surface of the specimen was coated with a thin layer of heavy metal. A new surface for serial block-face imaging was generated using a 3View in-chamber ultramicrotome (Gatan) within a SIGMA/VP SEM (Carl Zeiss Microscopy, Jena, Germany). Block-face images were obtained every 70-nm depth with a backscattered electron detector at an acceleration voltage of 1.1 kV. The pixel size was 21.0 nm/pixel wide, 21.0 nm/pixel height, 70 nm/pixel depth, and the pixel dimensions of a recorded image were 4096×4096 pixels. The contrast of the images was inversed.

Data processing for three-dimensional reconstruction

Segmentation and three-dimensional reconstruction of podocytes were performed using AMIRA 6.0 Software (FEI Visualization Science Group, Burlington, MA, USA) for both FIB-SEM and SBF-SEM data. The segmentation and extraction of podocytes from the block-face images was easily performed because these images were quite similar to conventional TEM images and exhibited enough high contrast to identify the three types of glomerular cells, mesangial matrix and GBM.

Acknowledgements

The data collection by SBF-SEM was supported by the collaborative research program of National Institute for Physiological Sciences. A part of data collection by FIB-SEM was supported by Nagoya University microstructural characterization platform as a program of 'Nanotechnology Platform' of the Ministry of Education, Culture, Sports, Science, and Technology of Japan. The authors wish to thank Takanobu Ishimura (Maxnet Co., Ltd., Tokyo, Japan) for the technical lecture on the three-dimensional reconstruction.

Competing interests

The authors declare no competing or financial interests.

Author contributions

K.I. designed the experiments. K.I., S.K., N.M., S.E., S.A. and K.M. obtained serial block-face SEM images. K.I., S.K., Y.K., T.M., T.N. performed three-dimensional reconstruction. K.I., M.K. and T.S. analyzed the experimental data. K.I. prepared the figures and wrote the manuscript.

Funding

This study was supported in part by a Grant-in-Aid for Scientific Research from the Ministry of Education, Culture, Sports, Science, and Technology (MEXT) [grant number 15K18960 to K.I.]; and Grants-in-Aid from the Foundation of Strategic Research Projects in Private Universities from MEXT [grant numbers S1311011, S1101009 to Juntendo University]. Deposited in PMC for immediate release.

Supplementary information

Supplementary information available online at
http://jcs.biologists.org/lookup/doi/10.1242/jcs.187815.supplemental

References

Andrews, P. M. and Porter, K. R. (1974). A scanning electron microscopic study of the nephron. *Am. J. Anat.* **140**, 81-115.

Bulger, R. E., Siegel, F. L. and Pendergrass, R. (1974). Scanning and transmission electron microscopy of the rat kidney. *Am. J. Anat.* **139**, 483-501.

Burghardt, T., Hochapfel, F., Salecker, B., Meese, C., Gröne, H. -J., Rachel, R., Wanner, G., Krahn, M. P. and Witzgall, R. (2015). Advanced electron microscopic techniques provide a deeper insight into the peculiar features of podocytes. *Am. J. Physiol. Renal. Physiol.* **309**, F1082-F1089.

Denk, W. and Horstmann, H. (2004). Serial block-face scanning electron microscopy to reconstruct three-dimensional tissue nanostructure. *PLoS Biol.* **2**, e329.

Dong, H.-M., Ichimura, K. and Sakai, T. (2010). Structural organization of hepatic portal vein in rat with special reference to musculature, intimal folds, and endothelial cell alignment. *Anat. Rec.* **293**, 1887-1895.

Fujita, T., Tokunaga, J. and Miyoshi, M. (1970). Scanning electron microscopy of the podocytes of renal glomerulus. *Arch. Histol. Jpn.* **32**, 99-113.

Furuse, M., Izumi, Y., Oda, Y., Higashi, T. and Iwamoto, N. (2014). Molecular organization of tricellular tight junctions. *Tissue Barriers* **2**, e28960.

Garrod, D. R. and Fleming, S. (1990). Early expression of desmosomal components during kidney tubule morphogenesis in human and murine embryos. *Development* **108**, 313-321.

Georgas, K., Rumballe, B., Valerius, M. T., Chiu, H. S., Thiagarajan, R. D., Lesieur, E., Aronow, B. J., Brunskill, E. W., Combes, A. N., Tang, D. et al. (2009). Analysis of early nephron patterning reveals a role for distal RV proliferation in fusion to the ureteric tip via a cap mesenchyme-derived connecting segment. *Dev. Biol.* **332**, 273-286.

Hartleben, B., Widmeier, E., Wanner, N., Schmidts, M., Kim, S. T., Schneider, L., Mayer, B., Kerjaschki, D., Miner, J. H., Walz, G. et al. (2012). Role of the polarity protein Scribble for podocyte differentiation and maintenance. *PLoS ONE* **7**, e36705.

Hay, D. A. and Evan, A. P. (1979). Maturation of the glomerular visceral epithelium and capillary endothelium in the puppy kidney. *Anat. Rec.* **193**, 1-21.

Heymann, J. A. W., Hayles, M., Gestmann, I., Giannuzzi, L. A., Lich, B. and Subramaniam, S. (2006). Site-specific 3D imaging of cells and tissues with a dual beam microscope. *J. Struct. Biol.* **155**, 63-73.

Higashi, T., Tokuda, S., Kitajiri, S.-i., Masuda, S., Nakamura, H., Oda, Y. and Furuse, M. (2013). Analysis of the 'angulin' proteins LSR, ILDR1 and ILDR2–tricellulin recruitment, epithelial barrier function and implication in deafness pathogenesis. *J. Cell Sci.* **126**, 966-977.

Ichimura, K. and Sakai, T. (2015). Evolutionary morphology of podocytes and primary urine-producing apparatus. *Anat. Sci. Int.* doi:10.1007/s12565-015-0317-7.

Ichimura, K., Kurihara, H. and Sakai, T. (2007). Actin filament organization of foot processes in vertebrate glomerular podocytes. *Cell Tissue Res.* **329**, 541-557.

Ichimura, K., Kurihara, H. and Sakai, T. (2010). Primary cilia disappear in rat podocytes during glomerular development. *Cell Tissue Res.* **341**, 197-209.

Ichimura, K., Miyazaki, N., Sadayama, S., Murata, K., Koike, M., Nakamura, K.-i., Ohta, K. and Sakai, T. (2015). Three-dimensional architecture of podocytes revealed by block-face scanning electron microscopy. *Sci. Rep.* **5**, 8993.

Iino, N., Gejyo, F., Arakawa, M. and Ushiki, T. (2001). Three-dimensional analysis of nephrogenesis in the neonatal rat kidney: light and scanning electron microscopic studies. *Arch. Histol. Cytol.* **64**, 179-190.

Ikenouchi, J., Furuse, M., Furuse, K., Sasaki, H. and Tsukita, S. (2005). Tricellulin constitutes a novel barrier at tricellular contacts of epithelial cells. *J. Cell Biol.* **171**, 939-945.

Inokuchi, S., Shirato, I., Kobayashi, N., Koide, H., Tomino, Y. and Sakai, T. (1996). Re-evaluation of foot process effacement in acute puromycin aminonucleoside nephrosis. *Kidney Int.* **50**, 1278-1287.

Iwamoto, N., Higashi, T. and Furuse, M. (2014). Localization of angulin-1/LSR and tricellulin at tricellular contacts of brain and retinal endothelial cells in vivo. *Cell Struct. Funct.* **39**, 1-8.

Knott, G., Marchman, H., Wall, D. and Lich, B. (2008). Serial section scanning electron microscopy of adult brain tissue using focused ion beam milling. *J. Neurosci.* **28**, 2959-2964.

Knott, G., Rosset, S. and Cantoni, M. (2011). Focussed ion beam milling and scanning electron microscopy of brain tissue. *J. Vis. Exp.*, e2588.

Koda, R., Zhao, L., Yaoita, E., Yoshida, Y., Tsukita, S., Tamura, A., Nameta, M., Zhang, Y., Fujinaka, H., Magdeldin, S. et al. (2011). Novel expression of claudin-5 in glomerular podocytes. *Cell Tissue Res.* **343**, 637-648.

Kriz, W. and Kaissling, B. (2000). Structural organization of the mammalian kidney. In *The Kidney, Physiology and Pathophysiology* (ed. D. W. Seldin and G. Giebisch), pp. 587-654. Philadelphia: Lippincott Williams & Wilkins.

Kubota, Y. (2015). New developments in electron microscopy for serial image acquisition of neuronal profiles. *Microscopy* **64**, 27-36.

Little, M. H., Brennan, J., Georgas, K., Davies, J. A., Davidson, D. R., Baldock, R. A., Beverdam, A., Bertram, J. F., Capel, B., Chiu, H. S. et al. (2007). A high-resolution anatomical ontology of the developing murine genitourinary tract. *Gene Expr. Patterns* **7**, 680-699.

Miyoshi, M., Fujita, T. and Tokunaga, J. (1971). The differentiation of renal podocytes. A combined scanning and transmission electron microscope study in rats. *Arch. Histol. Jpn.* **33**, 161-178.
Neal, C. R., Crook, H., Bell, E., Harper, S. J. and Bates, D. O. (2005). Three-dimensional reconstruction of glomeruli by electron microscopy reveals a distinct restrictive urinary subpodocyte space. *J. Am. Soc. Nephrol.* **16**, 1223-1235.
Nguyen, H. B., Thai, T. Q., Saitoh, S., Wu, B., Saitoh, Y., Shimo, S., Fujitani, H., Otobe, H. and Ohno, N. (2016). Conductive resins improve charging and resolution of acquired images in electron microscopic volume imaging. *Sci. Rep.* **6**, 23721.
Ohno, N., Katoh, M., Saitoh, Y., Saitoh, S. and Ohno, S. (2015). Three-dimensional volume imaging with electron microscopy toward connectome. *Microscopy* **64**, 17-26.
Ohta, K., Sadayama, S., Togo, A., Higashi, R., Tanoue, R. and Nakamura, K. (2012). Beam deceleration for block-face scanning electron microscopy of embedded biological tissue. *Micron* **43**, 612-620.
Patrakka, J. and Tryggvason, K. (2010). Molecular make-up of the glomerular filtration barrier. *Biochem. Biophys. Res. Commun.* **396**, 164-169.
Quaggin, S. E. and Kreidberg, J. A. (2008). Development of the renal glomerulus: good neighbors and good fences. *Development* **135**, 609-620.
Reeves, W., Caulfield, J. P. and Farquhar, M. G. (1978). Differentiation of epithelial foot processes and filtration slits: sequential appearance of occluding junctions, epithelial polyanion, and slit membranes in developing glomeruli. *Lab. Invest.* **39**, 90-100.
Rodewald, R. and Karnovsky, M. J. (1974). Porous substructure of the glomerular slit diaphragm in the rat and mouse. *J. Cell Biol.* **60**, 423-433.
Scott, R. P. and Quaggin, S. E. (2015). Review series: The cell biology of renal filtration. *J. Cell Biol.* **209**, 199-210.
Sonomura, T., Furuta, T., Nakatani, I., Yamamoto, Y., Unzai, T., Matsuda, W., Iwai, H., Yamanaka, A., Uemura, M. and Kaneko, T. (2013). Correlative analysis of immunoreactivity in confocal laser-scanning microscopy and scanning electron microscopy with focused ion beam milling. *Front. Neural Circuits* **7**, 26.
Spinelli, F. (1974). Structure and development of the renal glomerulus as revealed by scanning electron microscopy. *Int. Rev. Cytol.* **39**, 345-378.
Takahashi-Iwanaga, H. (2002). Comparative anatomy of the podocyte: A scanning electron microscopic study. *Microsc. Res. Tech.* **57**, 196-202.
Usui, J., Kurihara, H., Shu, Y., Tomari, S., Kanemoto, K., Koyama, A., Sakai, T., Takahashi, T. and Nagata, M. (2003). Localization of intercellular adherens junction protein p120 catenin during podocyte differentiation. *Anat. Embryol.* **206**, 175-184.
Yaoita, E., Sato, N., Yoshida, Y., Nameta, M. and Yamamoto, T. (2002a). Cadherin and catenin staining in podocytes in development and puromycin aminonucleoside nephrosis. *Nephrol. Dial. Transplant.* **17** Suppl. 9, 16-19.
Yaoita, E., Yao, J., Yoshida, Y., Morioka, T., Nameta, M., Takata, T., Kamiie, J.-i., Fujinaka, H., Oite, T. and Yamamoto, T. (2002b). Up-regulation of connexin43 in glomerular podocytes in response to injury. *Am. J. Pathol.* **161**, 1597-1606.